Enzyme Conformation Influences the Performance of Lipase-powered Nanomotors

Lei Wang,[a,b] Marzia Marciello,[c] Miquel Estévez-Gay,[d] Paul E.D. Soto Rodriguez,[b] Yurena Luengo Morato,[c] Javier Iglesias-Fernández,[d] Xin Huang,[a] Sílvia Osuna,[d,e] Marco Filice,*[c,f] and Samuel Sánchez *[b,e]

[a] Dr. L. Wang, Prof. Dr. X. Huang, MIIT Key Laboratory of Critical Materials Technology for New Energy Conversion and Storage, School of Chemistry and Chemical Engineering, Harbin Institute of Technology, Harbin 150001, China.
[b] Dr. L. Wang, Dr. P.E.D.S. Rodriguez, Prof. Dr. S. Sanchez, Institute for Bioengineering of Catalonia (IBEC), The Barcelona Institute of Science and Technology (BIST), Baldiri i Reixac 10-12, 08028 Barcelona, Spain. E-mail: ssanchez@ibecbarcelona.eu
[c] Dr. M. Marciello, Dr. Y.L. Morato, Dr. M. Filice, Nanobiotechnology for Life Sciences Lab, Department of Chemistry in Pharmaceutical Sciences, Faculty of Pharmacy, Complutense University of Madrid (UCM), Plaza Ramón y Cajal, 28040 Madrid, Spain. E-mail: mfilice@ucm.es
[d] Dr. M. Estevez-Gay, Dr. J.I. Fernandez, Dr. S. Osuna, Compbiolab Group, Institut de Química Computacional i Catàlisi (IQCC) and Departament de Química, Universitat de Girona, carrer Maria Aurelia Capmany 69, 17003 Girona, Spain.
[e] Prof. Dr. S. Sanchez, Dr. S. Osuna, Institució Catalana de Recerca i Estudis Avançats (ICREA), Pg. Lluís Companys 23, 08010 Barcelona, Spain.
[f] Dr. M. Filice, Microscopy and Dynamic Imaging Unit, Fundación Centro Nacional de Investigaciones Cardiovasculares Carlos III (CNIC), Calle Melchor Fernandez Almagro 3, E-28029 Madrid, Spain.

Supporting information for this article is given via a link at the end of the document.

Abstract: Enzyme powered micro/nanomotors have great potential applications in various areas. To efficiently reach those applications, it is necessary to understand the fundamental aspects affecting the motion dynamics. Herein, we explored the impact of enzyme orientation on the performance of lipase-powered nanomotors by tuning the lipase immobilization strategies. The influence of the lipase orientation and lid conformation on substrate binding and catalysis was analyzed *via* MD simulations. Besides, the motion performance indicates the hydrophobic binding (*via* OTES) represents the best orienting strategy, providing 48.4 % and 95.4% increase in diffusion coefficient compared to hydrophilic binding (*via* APTES) and Brownian motion (no fuel) respectively (with $C_{[triacetin]}$ of 100 mM). This work provides critical evidences of immobilization strategy and corresponding enzyme orientation for the catalytic activity and in turn, the motion performance of nanomotors, thus helpful to future applications.

Introduction

The past two decades has witnessed the tremendous advancements of micro- and nanomotors in various research fields, especially in biomedical[1] and environmental[2] areas. Catalytic micro/nanomotors are based on the conversion of chemical energy into a mechanical force[3], thus leading to active motion. Enzymes, conducting energy conversion in biosystems, are good candidates for the engines of micro/nanomotors[4], due to their inherent characteristics such as biocompatibility and highly efficient catalysis[5]. Hence, several enzymes have been investigated in the preparation of micro/nanomotors, including catalase[6], urease[7], and glucose oxidase[8], acetylcholinesterase (AChE) [9], trypsin[10], lipase[11], or multi-enzyme combination[12]. Albeit the fast advances of enzyme powered micro/nanomotors towards in vitro/vivo applications[13], the fundamental question of how catalytic processes impact on the motion performance of nanomotors remains unclear. To address this issue, Sanchez's group has clarified several basic questions, including the influences caused by enzyme poisoning and reactivation[14], the enzyme quantity and distribution[15], and the flexibility near the active site for different enzymes[9]. However, there are still several questions remaining to be solved, for instance how the enzyme orientation impacts on their catalytic efficiency, and hence on the resulting motion performance of micro/nanomotors.

In this regard, lipases (triacylglycerol ester hydrolases EC 3.1.1.3) are ideal candidates to address the above question. Up to 2017, lipases accounted for the third biggest category based on total global sales[16], with prevalent applications in both industrial and biotechnology areas.[17] Furthermore, thanks to their intrinsic characteristics (e.g. broad specificity, good stability and unique structure), lipases are expected to show potential functions in pharmaceutical and biomedical fields in the coming years. Recently, lipase has been used as engine for nanomotors and demonstrated the efficient degradation of triglyceride in vitro[11], which not only further expanded the enzyme library for biocompatible engines of nanomotors, but also provided potential biomedical and environmental applications. More significantly, within the enzyme realm, lipase presents a unique catalytic mechanism, characterized by the presence of a mobile subdomain lid or flap located over the active site.[18] Therefore, depending on the lipase surrounding environment, the lid can shift to seclude the catalytic site entrance or not, thus hampering or permitting the free diffusion of lipase substrates. In other terms, the lipase structure can shift between an open-active or close-inactive conformation depending on the lid movement.[19] This equilibrium could be well controlled by means of the immobilization strategy and supporting materials[20], thereby providing a good amphiphilic model to investigate the orientation effect on the motion behaviors of lipase-powered motors.

Herein, we study the effect of lipase orientation on the catalytic and mobility performance of lipase-powered nanomotors, both experimentally and by molecular dynamics (MD) simulations. Lipase from Candida rugosa (CRL) was immobilized on mesoporous silica nanoparticles (MSNs) through

three different interactions, namely ionic adsorption, glutaraldehyde-mediated covalent bonding, and hydrophobic interaction, providing different lipase conformation and orientations on MSNs (Supplementary Figure S1), which was confirmed by FTIR-ATR. Last but not least, both the catalytic efficiency and motion performance demonstrated that the lid opening mechanism could be achieved via controlled immobilization approaches, therefore providing a method for improving the performance of lipase powered nanomotors. Taken together, these results not only provide deep insights into the fundamental understanding of how the lipase orientation and manipulation influence the lipase-powered nanomotors, but also to offer a guidance for future preparation of more efficient nanomotors, towards promoting the potential biomedical or environmental applications.

Results and Discussion

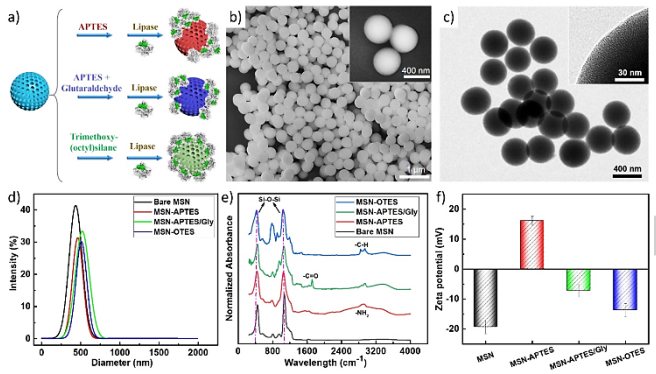

Figure 1. (a) Scheme of the synthesis of MSNs, and following modification using three different protocols, including i) 3-aminopropyltriethoxysilane (APTES), ii) APTES + glutaraldehyde (APTES/GLY), iii) trimethoxy-(octyl)silane (OTES). (b-c) SEM and TEM images showing the produced MSNs, with high resolution images inset. (d-f) DLS, FTIR and Zeta potential results, showing the size, surface functional groups and surface charges of the MSNs, after modification using different silanes.

In this study, MSNs were selected as the supporting material for the immobilization of lipase, due to the easily tuning of their surface charges and functional groups (Figure 1a).[21] Based on dynamic light scattering characterization (DLS, Figure 1d), the synthesized MSNs consisted of uniform spherical porous structures (Figure 1b-c), with an average diameter of 413.28±2.77 nm (N=150) and a polydispersity index of 0.27. In order to obtain MSNs with different surface functional groups, three different silanes was adopted for the modification, thus obtaining three types of supporting MSNs with amino groups, aldehyde groups, and hydrocarbyl groups respectively (Figure 1e), thus resulting in three corresponding interactions for the following modification of lipase, namely ionic adsorption (MSN-APTES), covalent bonding (MSN-APTES/GLY), and hydrophobic interaction (MSN-OTES). FTIR was firstly conducted to confirm the different modification (Figure 1e), showing the representative peaks from each silane. From the plots, we can see the peaks that appear at 400 cm^{-1} are attributed to the bending vibration of Si-O-Si bond, and the peaks shown at 800 and 1080 cm^{-1} are due to the symmetric and asymmetric stretching vibration of Si-O-Si bonds, confirming the existence of MSNs respectively. Furthermore, the peaks at 2850/2940 cm^{-1} (C-H stretching vibration), 1700 cm^{-1} (C=O stretching vibration), 3000 cm^{-1} (N-H stretching vibration) confirmed the existence of three different silanes on the surface of MSNs. The successful modification using different silanes was also proved by the change of surface charge (Figure 1f): the as-synthesized MSNs had a negative surface charge of -19.36±2.15 mV, which increased up to 16.15±1.43 mV after amination. Similarly, after the modification with glutaraldehyde, the surface charge decreased back to a slight negative value (-7.2±2.15 mV). The modification with OTES kept the surface of MSNs at negative state of -13.7±2.27 mV. After each modification step, there was still only one single population distribution in the hydrodynamic radius plots (Figure 1d), even after lipase modification (Supplementary Figure S2), demonstrating excellent dispersity of MSNs in solution. The increase in hydrodynamic radius and the broader peak can be attributed to the attachment of silanes. Once prepared and characterized, the three types of MSNs were used for the different immobilization strategies, to achieve the different orientations of CRL on each silica surface.

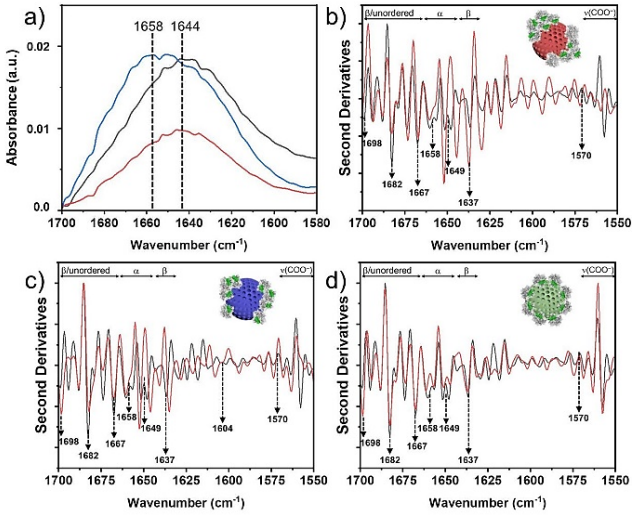

Figure 2. Structural characterization of CRL-powered nanomotors. a) FTIR-ATR spectra in the amide I region of CRL lipase immobilized on MSN-APTES (black line), MSN-APTES/GLY (red line) and MSN-OTES (blue line); b) Second derivative of amide I band for free lipase (black line) and lipase immobilized on MSN-APTES (red line); c) Second derivative of amide I band for free lipase (black line) and lipase immobilized on MSN-APTES/GLY (red line); d) Second derivative of amide I band for free lipase (black line) and lipase immobilized on MSN-OTES (red line).

It is well-known that the activity of an enzyme is strongly dependent on its secondary structure as well as its complete 3D structure[22], which is influenced by the chemical and physical properties of the supporting material. Infrared spectroscopy is a well-established technique for the conformational analysis of proteins especially upon their immobilization on solid supports[23], and thanks to the attenuated total reflectance (ATR) technique[24], protein absorption bands can be obtained with a good signal-to-noise ratio at a low concentration[25]. As reported previously[26], the analysis of the amide I absorption in the 1700–1550 cm^{-1} region is the best choice to obtain relevant information on the secondary structure elements of lipase. Hence, considering that

the amide I band (due to the C=O stretching vibration coupled with an out-of-phase C–N stretching and C–C–N deformation of the peptide backbone) [27] is more conformational sensitive because of its frequency dependence on the hydrogen-bonding and coupling along the protein chain, we decided to focus on that zone in each spectra with the aim to analyze the protein conformation as a function of each immobilization strategy. [28]

The spectra of amide I band of CRL immobilized on each different MSNs is obtained (Figure 2a and Figure S3). CRL immobilized on MSN-APTES and MSN-APTES/GLY exhibited similar amide I bands profile and maximum value (1644 cm^{-1}). However, CRL@MSN-OTES showed a clear shift of the amide I band toward higher wavenumber (1658 cm^{-1}), implying a different structure conformation assumed by the lipase when immobilized on this more hydrophobic material (Figure 2a). To clarify the impact of different MSNs on the lipase orientation, the second derivative of the amide I spectra of each enzyme derivative was calculated (Figure2b-d). The amide I components of free CRL were then assigned to the different secondary structure elements according to previous studies[29], which are in good agreement with the analysis of its crystal structure by X-ray diffraction. [19c]

As described in literature, the components comprised in the 1610-1590 cm^{-1} spectral range can be attributed to strongly hydrogen bonded intermolecular β-sheets structures.[24] Within this range, in comparison with free CRL in solution (24%), the second derivative of three lipase-nanomotors shows a relative intensity loss in all cases. Nonetheless, if compared within them, the second derivative values of lipase derivatives showed clear differences as a function of the immobilization protocol. In more details, CRL@MSN-APTES (Figure 2b) and CRL@MSN-APTES/GLY (Figure 2c) spectra show 13.86% and 15.28% intensity, respectively, whereas in the case of CRL@MSN-OTES (Figure 2d) a clear loss of relative intensity of the bands comprised in that zone can be appreciated (11.84%). As general consideration, these results indicate that the lipase molecules are less aggregated in comparison with free CRL because of the immobilization on the MSN nanoparticles. In more details, the comparison within immobilized lipases indicates that CRL molecules immobilized on OTES surface present a less intermolecular interaction between them. Thus, this evidence clearly indicates that the lipase has been immobilized on the MSNs hydrophobic surface in a less aggregated manner and with a more homogeneous distribution in comparison with the other two cases.

Comparing the reference components of free CRL with those of immobilized CRL on each type of MSN, in the case of CRL@MSN-OTES (Figure 2d), the intensity of the bands in the spectral range of organized α-helix (region with bands centered at 1658 and 1649 cm^{-1} and the main component of lid in its close conformation[19c]) decreased (42.2% *vs* 26.58% of free CRL and CRL@MSN-OTES, respectively; Supporting Table 1) while the bands related to disordered structure (1665–1700 cm^{-1}) exhibited a clear relative increase (21.13% *vs* 29.49% of free CRL and CRL@MSN-OTES, respectively; Supporting Table 1). This behavior is consistent with a previous report that described one part of α-helix of lipase transformed into less ordered elements, when CRL was incorporated into hydrophobic microenvironment.[30] This structural change can be explained by the transition of the lid from close to open conformation as a consequence of the catalytic site opening, thus confirming that the most active conformation of CRL was achieved and 'frozen' on the surface of supporting materials because of the presence of hydrophobic layer (hydrocarbyl groups). Therefore, these results demonstrate that CRL has been immobilized onto the hydrophobic MSN-OTES in its open-active structural conformation (Supplementary Figure S1a).

To analyze the secondary structure of CRL immobilized on MSN-APTES, we focused our attention on the evaluation of the relationship between the bands within 1550 and 1575 cm^{-1} assigned to deprotonated υ(COO^-) belonging to side chains of glutamic and aspartic acid amino acids (Glu and Asp) and compared to the total area of amide I (comprised within 1550-1700 cm^{-1}, Figure 2b). Consequently, by analyzing the spectrum (1550-1570 cm^{-1}), we observed that the relative intensity of the deprotonated amino acid Glu and/or Asp peaks for CRL@MSN-APTES decreased notably (27.96% *vs* 13.82% of free CRL and CRL@MSN-APTES, respectively; Supporting Table 1, Figure 2b). These results indicate that during the immobilization on cationic MSN-APTES, at the immobilization pH (neutral), CRL adsorbs on the MSN surface through the negatively charged COO^- side chains by forming hydrogen bonds and/or by protonation with the NH_3^+ groups of APTES. Furthermore, the β-sheet/unordered zones do not change whilst the α-helices signals slightly increased in intensity (42.24% *vs* 44.4% of free CRL and CRL@MSN-APTES, respectively; Supporting Table 1) indicating that the related closed/inactive conformation of CRL (typical of free CRL enzyme in aqueous solutions) is mostly present in this enzyme derivative, thereby confirming the ionic interaction during the immobilization of CRL on MSN-APTES with the final bonding of the closed-inactive form of CRL (Supplementary Figure S1b).

Finally, for the case of CRL@MSN-APTES/GLY (Figure 2c), it is possible to observe the appearance of a shoulder at 1604 cm^{-1} (with higher intensity in comparison of bare MSN-APTES/GLY (data not shown)) that can be assigned to the imine bond υ(N=C) as a result of the reaction of residual aldehyde group of GA with amine groups of CRL (proceeding from the lysine side chains) as a result of the Schiff's base formation. Furthermore, an additional contribution of hydrophobic α-helix bands intensity decrease (42.24% vs 38.26% of free CRL and CRL@MSN-APTES/GLY, respectively; Supporting Table 1) with a concomitant increase of disordered structures within 1665–1700 cm^{-1}, (21.13% vs 28.11% of free CRL and CRL@MSN-APTES/GLY, respectively; Supporting Table 1) as well as ionic interaction (clear lowering of the bands intensities of the spectrum within 1550 and 1575 cm^{-1}: 27.96% *vs* 19.19% of free CRL and CRL@MSN-APTES/GLY, respectively; Supporting Table 1). Taken together, these results indicate that CRL was immobilized *via* a mix of ionic interaction, hydrophobic

adsorption and covalent bonding through glutaraldehyde linker on MSNs (Supplementary Figure S1c).

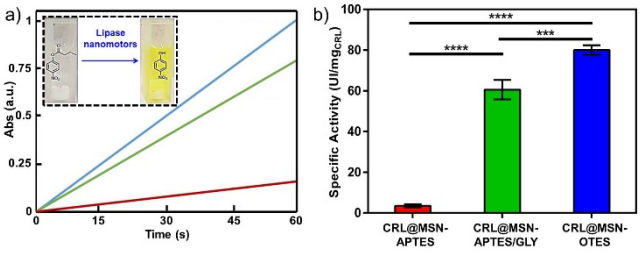

Figure 3 Catalytic characterization of different CRL@MSN nanomotors. a) Time course assessment of model substrate hydrolysis catalyzed by CRL@MSN-APTES (red line), CRL@MSN-APTES/GLY (green line) and CRL@MSN-OTES (blue line). The inset photos showing the sample solution before and after the catalytic reaction of CRL-powered motors; b) specific activity for each milligram of CRL immobilized on the different MSNs. Significance was calculated by one-way ANOVA test. ***: $p < 0.001$ or high significant statistical difference between the groups of data; ****: $p < 0.0001$ or very high significant statistical difference between the groups of data.

To characterize the catalytic property of each kind of CRL@MSN nanomotors, an enzymatic assay was carried out. This reaction is based on the time-dependent colorimetric evaluation of the appearance of colored 4-nitrophenol molecule, which is the hydrolysis product of uncolored 4-nitrophenyl butyl ester (model substrate of CRL) (Figure 3). In Figure 3a, with the same amount of CRL@MSN nanomotors and substrate, it is easily to observe that CRL@MSN-OTES performed best, with the highest efficiency (blue line in Figure 3a). By normalizing the kinetic results for each milligram of CRL immobilized on each nanomotor and quantified by the BCA assay (Figure 3b), it is possible to assess the real impact of each immobilization protocol on the CRL activity. The results indicated that the least active nanomotor was CRL@MSN-APTES (3.5 UI/mg$_{CRL}$), and CRL@MSN-OTES (78.5 UI/mg$_{CRL}$) was the most active one (Figure 3b), with CRL@MSN-APTES/GLY (60.5 UI/mg$_{CRL}$) in the middle, thus proving CRL immobilized *via* hydrophobic adsorption is the most active form. In order to further elucidate and correlate the impact of each immobilization protocol on the catalytic activity of CRL while normalizing all the other parameters (e.g. immobilized CRL amount), we carried out a kinetic study with the aim to calculate the Michaelis-Menten constant (*Km*) and the maximum initial velocity (*Vmax*) parameters (Supporting Figure S4). Especially the Km is a very useful parameter since it relates to the enzyme affinity to substrate (or binding affinity) and a high value of *Km* specifies a weak affinity.[31] The achieved experimental data (*Km* CRL@MSN-OTES: 0.4 mM < *Km* CRL@MSN-APTES/GLY: 0.45 < *Km* CRL@MSN-APTES 1.19 mM; Supporting Table S2) demonstrate the enhanced affinity of the substrate to the lipase immobilized by the interfacial activation mechanism. This higher substrate affinity is mainly due to the oriented immobilization of CRL in its open-active form on MSN-OTES surface and to the successful generation of the wide hydrophobic environment in the surroundings of CRL active center. Furthermore, the significantly higher *Vmax* value of CRL@MSN-OTES (202 U/mg) than that of the other two lipase-powered nanomotors (123 and 7.5 U/mg for CRL@MSN-APTES/GLY and CRL@MSN-APTES, respectively) indicates highly improved catalytic efficiency (Supporting Table S2). These results agreed well with the structural analysis proved using FTIR-ATR and the specific activity characterization discussed in the previous sections.

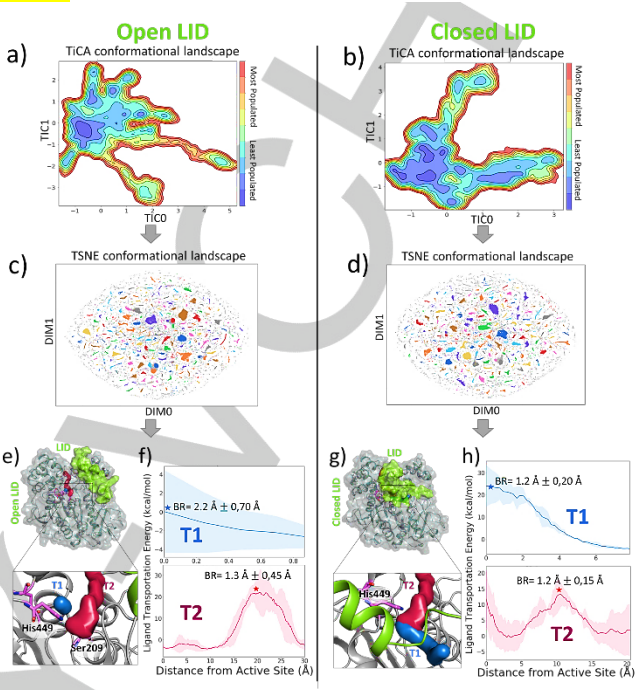

Figure 4. Scheme of the MD analysis process and substrate binding accessibility profiles. The dataset obtained from multiple MD simulations for open and closed CRL was reduced using a two-step process: first, the dimensionality reduction technique TICA was applied (TIC0 and TIC1 shown in a) and b) for open and closed CRL, most populated regions are displayed in blue, whereas less populated in red), which was further reduced into a 2D dimension with t-SNE (c-d), and clustered with HDBSCAN method. Each cluster in the t-SNE plots is coloured differently. The 4 most populated clusters were subjected to tunnel and ligand binding analysis. Representative open (e) and closed (g) CRL conformations adopted during the MD simulations are represented as cartoons. LID domain is shown in green, active site residues in purple sticks, and tunnel T1 and T2 in blue and raspberry solid surfaces, respectively. Ligand transportation energy profiles (f, h) computed from the most populated clusters after t-SNE reduction. The mean energy profile for substrate accessibility to the active site computed on multiple MD snapshots is shown with a solid line, and the standard deviation using a shaded region. Mean energy profiles for substrate accessibility through T1 and T2 tunnels are shown in blue and raspberry, respectively. The mean tunnel bottleneck radius (BR, marked with coloured stars in f-h, in Angstroms) together with the standard deviation is also shown.

As stated above, depending on the immobilization conditions applied in the experimental assays, CRL is immobilized with the lid domain either in a closed or open conformation, finally impacting on the lipase activity and thus potentially the propulsion of CRL@MSNs nanomotors. To further clarify how the lid conformation affects the lipase activity, we performed molecular dynamics (MD) simulations coupled to substrate access tunnel calculations with CaverDock[32] (see Figure 4). MD simulations starting from either open (Figure 4e) or closed conformations (Figure 4g) of the lid domain of CRL were performed with an accumulated MD simulation time of 6100 ns

(see computational details in SI). The opening and closing transitions of the lid were not sampled in any of the replicas, *i.e.* simulations starting from open state remained in the open state, in line with the relatively slow timescale of the conformational change of the lid domain in water. [33] In contrast, additional MD simulations performed at 100mM triacetin revealed a higher flexibility of the lid, which was able to transition from closed to partially open conformations (see Supplementary Figure S5). The performed MD simulations were further analyzed by means of dimensionality reduction techniques (see Figure 4 a-d, Figure S6 and full computational details in SI), to provide an ensemble of open and closed conformations of the lid domain of CRL for characterizing its impact on CRL catalytic efficiency and CRL@MSN propulsion. To that end, substrate accessibility was estimated through the calculation of access tunnels, tunnel bottleneck radius (BR), and evaluation of the associated energy barriers for substrate binding to the active site (see Figure 4f-h). For the ensemble of open CRL conformations, two tunnels were identified (Figure 4e, f): the wide T1 tunnel observed in 94% of analyzed open MD structures with a mean BR of 1.28 ± 0.24 Å, and the narrower T2 (BR of 1.04 ± 0.12 Å). Energy barriers associated to substrate binding into the active site indicate that the wider T1 tunnel is kinetically favored (barrier of ca. 2 kcal/mol), as a result of its short length and exposure to the solvent (see Figure 4f). In contrast, the narrower T2 has a substantially higher barrier for triacetin binding (*ca.* 26.3 kcal/mol). Interestingly, the same analysis performed on the set of closed CRL conformations (see Figure 4g) indicated that T1/T2 tunnels are detected at a lower rate (48%/39% of sampled MD conformations, respectively), and most importantly they are characterized by a slightly narrower BR (1.10 ± 0.20 Å for T1 and 1.01 ± 0.11Å for T2). These narrow T1 and T2 tunnels found in closed CRL conformations also present high energy barriers associated to triacetin binding (the estimated barriers are ca. 28.8 for T1 and 13.3 kcal/mol for T2, see Figure 4d). These large energy barriers can be traced back to hydrophobic residues V86 (Valine 86) and F87 (Phenylalanine 87) from the lid domain that restrict active site accessibility in the closed conformation (see Figure S7). These findings indicate that the immobilization of CRL with the lid domain in closed conformations prevent triacetin access to the active site, thus hindering CRL catalytic activity and inhibiting CRL@MSN propulsion.

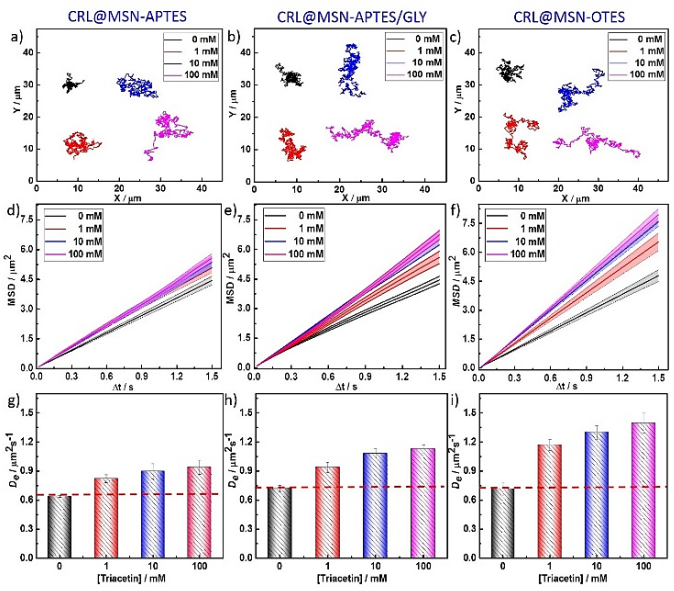

Figure 5 a-c) Representative trajectories (during 30s) of different lipase-powered MSNs nanomotors, in different triacetin concentrations (0, 1, 10, 100 mM), through different strategies: a) APTES, b) APTES/GLY, c) OTES. d-f) Mean square displacements (MSDs; n≥20, error bars represent Standard Error (SE)) corresponding to (a-c). g-i) Diffusion coefficients of different lipase-powered nanomotors obtained by analyzing the MSD (d-f) for different triacetin concentrations.

To fully understand the influences on motility behavior caused by the lipase orientation, we tested different concentrations of triacetin as fuel to trigger the motion of these three types of CRL@MSN nanomotors. The mean squared displacement (MSD, Figure 5d-f) was calculated from the tracked trajectories (Figure 5a-c), using a home-made python code, showing a linearly increase with time and fuel concentration, thus indicating a fuel-concentration-dependent motility, which is consistent with our previous findings[9,11]. The diffusion coefficient (*De*) was obtained from the MSD per time interval (Δt) as *De*=0.25 MSD/Δt. During the studied time range, the *De* value of lipase motors with APTES as linker was 0.64 $\mu m^2 s^{-1}$ in PBS solution with no triacetin, and increased to 0.82, 0.89 and 0.93 $\mu m^2 s^{-1}$, when 1, 10 and 100 mM triacetin was added, with the corresponding increase percentage of 28.6%, 40.7% and 47.0%, respectively (Figure 5g). This illustrates the increase of *De* values with fuel concentration. Similarly, for the lipase motors linked with glutaraldehyde, and OTES, the increase percentages of *De* values are 30.3%, 49.9%, 56.6% (Figure 5h) and 63.8%, 82.0%, 95.4% (Figure 5i), respectively. We could observe an increase of *De* values of lipase nanomotors when open conformation (hydrophobic binding) takes place, which is consistent with previous catalytic ability (Figure 3) and MD analysis (Figure 4). This enhanced motility behavior might be also due to the higher concentration of triacetin in the wide hydrophobic environment created in the lipase's catalytic site surroundings by the large hydrophobic pocket resulting from the open form of CRL and through OTES modification. Finally, we explored the stability of each nanomotor in the experimental conditions of motion analysis (Supplementary Figure S8). In all the cases, the CRL@MSN-OTES nanomotor showed higher stability in comparison with CRL@MSN-APTES/GLY and CRL@MSN-APTES, thus, demonstrating the positive impact of hydrophobic immobilization. Therefore, in this work, we can easily confirm the best orientation of lipase is based on the OTES strategy, providing almost one-fold increase of the *De* value compared to that of the Brownian motion. All these results show that the lipase orientation is a crucial parameter for tuning the motion behaviors, thereby providing a strategy for the preparation of efficient and stable enzyme-powered nanomotors, towards promoting their biomedical and environmental applications.

Conclusions

In this work, we demonstrated that the structural conformation and orientation of immobilized lipase play a key role in finely modulating and enhancing motility behavior of lipase-powered

nanomotors. Through different immobilization strategies, CRL was immobilized onto three different supporting platforms through ionic interaction, covalent bonding, and hydrophobic interaction, thus leading to fundamental conformation changes as a function of the different orientations and accessibility of the catalytic center. The correlation between structural analysis and catalytic characterizations together with molecular dynamics simulation confirmed that the oriented immobilization of CRL in its open conformation through hydrophobic adsorption was crucial for achieving the most efficient catalytic process and, consequently, the fastest and more stable nanomotor. Thus, the enzyme orientation strategy was revealed to be a crucial factor to modulate and enhance the diffusion coefficient of lipase-powered nanomotors. Therefore, this work does not only answer one of the basic questions of lipase-powered nanomotors, but also paves a way towards the creation of a fine modulating tool of enzyme powered motors, thereby expanding their potential applications in both biomedical and environmental fields.

Acknowledgements

L. W. thanks the NSFC (No. 51703043), the Marie Sklodowska-Curie Fellowship (Grant No. 712754), and the Severo Ochoa programme (Grant SEV-2014-0425(2015-2019)). X.H. appreciates the NSFC (No. 21871069). P.E.D.S.R acknowledges postdoctoral fellowship support from the Spanish MINECO “Juan de la Cierva formación” program 2016 FJCI-2016-29512. M.M, Y.L.M. and M.F. are grateful to the Comunidad Autonoma de Madrid and FEDER for the I+D collaborative Programme in Biomedicine NIETO-CM (Project reference B2017-BMD3731). S.O. thanks the Generalitat de Catalunya for the emerging group CompBioLab (No. 2017 SGR-1707), Spanish MINECO for project PGC2018-102192-B-I00, and the European Research Council (ERC) under the European Union’s Horizon 2020 research and innovation program (No. ERC-2015-StG-679001). J.I.F. acknowledges postdoctoral fellowship support from the Spanish MINECO “Juan de la Cierva formación” program IJCI-2017-34129, and the Marie Sklodowska-Curie Fellowship (H2020-MSCA-IF-2016-753045, J.I.F). M.F. thanks MINECO for the research grant No. SAF2014-59118-JIN co-funded by FEDER and also the Comunidad Autonoma de Madrid for research project No. 2017-T1/BIO-4992 (“Atracción de Talento” Action) co-funded by Universidad Complutense de Madrid. The CNIC is supported by MINECO and the Pro-CNIC Foundation and is a Severo Ochoa Centre of Excellence (SEV-2015-0505). S.S. thanks the Spanish MINECO for grants CTQ2015-68879-R (MICRODIA) and CTQ2015-72741-EXP (Enzwim), and Proyecto RTI2018-098164-B-I00 funded by MCIU/AEI/FEDER, UE. The authors would like to appreciate Joaquim Llacer for fruitful discussions.

Author Contributions

L.W., M.F. and S.S. conceived the idea, designed and lead the experiments. L.W. synthesized, modified and characterized the nanoparticles, also tracked, characterized and analyzed the motion behaviors of different nanomotors. M.M. carried out the CRL immobilization and the catalytic characterization of different nanomotors. Y.L.M carried out the FTIR-ATR characterization. M.E., J.F. and S.O. did the molecular dynamic simulations. L.W., P.E.D.S.R, X.H., M.F., S.S analyzed and discussed all the data. S.S. supervised the project. All authors contributed to the paper writing, revision and agreed with the final version.

Keywords: Micro/nanomotors • enzyme powered micro/nanomotors • lipase • molecular dynamics simulations • nanobiotechnology

[1] a) L. K. E. A. Abdelmohsen, F. Peng, Y. Tu, D. A. Wilson, *J. Mater. Chem. B* **2014**, *2*, 2395–2408; b) J. Wang, R. Dong, H. Wu, Y. Cai, B. Ren, *Nano-Micro Lett.* **2020**, *12*, 11; c) M. Luo, Y. Feng, T. Wang, J. Guan, *Adv. Funct. Mater.* **2018**, *28*, 1706100; d) W. Gao, J. Wang, *Nanoscale* **2014**, *6*, 10486–10494.

[2] a) W. Gao, J. Wang, *ACS Nano* **2014**, *8*, 3170–3180; b) B. Jurado-Sánchez, J. Wang, *Environ. Sci. Nano* **2018**, *5*, 1530–1544; c) J. Parmar, D. Vilela, K. Villa, J. Wang, S. Sánchez, *J. Am. Chem. Soc.* **2018**, *140*, 9317–9331.

[3] a) M. Safdar, S. U. Khan, J. Jänis, *Adv. Mater.* **2018**, *30*, 1703660; b) L. Wang, Y. Liu, J. He, M. J. Hourwitz, Y. Yang, J. T. Fourkas, X. Han, Z. Nie, *Small* **2015**, *11*, 3762–3767; c) L. Wang, S. Song, J. van Hest, L. K. E. A. Abdelmohsen, X. Huang, S. Sánchez, *Small* **2020**, 1907680; d) Y. Lin, L. Wang, X. Huang, *Chem. – A Eur. J.* **2019**, *25*, 16440–16450; e) Y. Wu, T. Si, C. Gao, M. Yang, Q. He, *J. Am. Chem. Soc.* **2018**, *140*, 11902–11905.

[4] S. Gáspár, *Nanoscale* **2014**, *6*, 7757–7763.

[5] a) T. Patiño, X. Arqué, R. Mestre, L. Palacios, S. Sánchez, *Acc. Chem. Res.* **2018**, *51*, 2662–2671; b) X. Zhao, K. Gentile, F. Mohajerani, A. Sen, *Acc. Chem. Res.* **2018**, *51*, 2373–2381.

[6] a) X. Ma, A. Jannasch, U.-R. Albrecht, K. Hahn, A. Miguel-López, E. Schäffer, S. Sánchez, *Nano Lett.* **2015**, *15*, 7043–7050; b) S. Sanchez, A. A. Solovev, Y. Mei, O. G. Schmidt, *J. Am. Chem. Soc.* **2010**, *132*, 13144–13145; c) A. Somasundar, S. Ghosh, F. Mohajerani, L. N. Massenburg, T. Yang, P. S. Cremer, D. Velegol, A. Sen, *Nat. Nanotechnol.* **2019**, *14*, 1129–1134; d) S. Ghosh, F. Mohajerani, S. Son, D. Velegol, P. J. Butler, A. Sen, *Nano Lett.* **2019**, *19*, 6019–6026.

[7] a) A. C. Hortelão, R. Carrascosa, N. Murillo-Cremaes, T. Patiño, S. Sánchez, *ACS Nano* **2019**, *13*, 429–439; b) A. C. Hortelão, T. Patiño, A. Perez-Jiménez, À. Blanco, S. Sánchez, *Adv. Funct. Mater.* **2018**, *28*, 1705086; c) K. K. Dey, X. Zhao, B. M. Tansi, W. J. Méndez-Ortiz, U. M. Córdova-Figueroa, R. Golestanian, A. Sen, *Nano Lett.* **2015**, *15*, 8311–8315.

[8] a) Y. Ji, X. Lin, Z. Wu, Y. Wu, W. Gao, Q. He, *Angew. Chemie Int. Ed.* **2019**, *58*, 12200–12205; b) P. Schattling, B. Thingholm, B. Städler, *Chem. Mater.* **2015**, *27*, 7412–7418.

[9] X. Arqué, A. Romero-Rivera, F. Feixas, T. Patiño, S. Osuna, S. Sánchez, *Nat. Commun.* **2019**, *10*, 2826.

[10] P. S. Schattling, M. A. Ramos-Docampo, V. Salgueiriño, B. Städler, *ACS Nano* **2017**, *11*, 3973–3983.

[11] L. Wang, A. C. Hortelão, X. Huang, S. Sánchez, *Angew. Chem. Int. Ed.* **2019**, *58*, 7992–7996.

[12] a) C. Gao, C. Zhou, Z. Lin, M. Yang, Q. He, *ACS Nano* **2019**, *13*, 12758–12766; b) L. K. E. A. Abdelmohsen, M. Nijemeisland, G. M. Pawar, G.-J. A. Janssen, R. J. M. Nolte, J. C. M. van Hest, D. A. Wilson, *ACS Nano* **2016**, *10*, 2652–2660; c) D. Pantarotto, W. R. Browne, B. L. Feringa, *Chem. Commun.* **2008**, 1533–1535; d) A. Joseph, C. Contini, D. Cecchin, S. Nyberg, L. Ruiz-Perez, J. Gaitzsch, G. Fullstone, X. Tian, J. Azizi, J. Preston, G. Volpe, G. Battaglia, *Sci. Adv.* **2017**, *3*, e1700362.

[13] a) J. Ou, K. Liu, J. Jiang, D. A. Wilson, L. Liu, F. Wang, S. Wang, Y. Tu, F. Peng, *Small* **2020**, 1906184; b) M. Medina-Sánchez, H. Xu, O. G. Schmidt, *Ther. Deliv.* **2018**, *9*, 303–316; c) K. Kim, J. Guo, Z. Liang, D. Fan, *Adv.*

Funct. Mater. **2018**, *28*, 1705867.
[14] X. Ma, X. Wang, K.Hahn, S. Sánchez, *ACS Nano* **2016**, *10*, 3597−3605.
[15] T. Patiño, N. Feiner-Gracia, X. Arqué, A. Miguel-López, A. Jannasch, T. Stumpp, E. Schäffer, L. Albertazzi, S. Sánchez, *J. Am. Chem. Soc.* **2018**, *140*, 7896–7903.
[16] A. . Srivastava, M. Srivastava, *Allied Mark. Res.* **2019**.
[17] a) D. G. Filho, A. G. Silva, C. Z. Guidini, *Appl. Microbiol. Biotechnol.* **2019**, *103*, 7399–7423; b) N. Sarmah, D. Revathi, G. Sheelu, K. Yamuna Rani, S. Sridhar, V. Mehtab, C. Sumana, *Biotechnol. Prog.* **2018**, *34*, 5–28.
[18] a) A. M. Brzozowski, U. Derewenda, Z. S. Derewenda, G. G. Dodson, D. M. Lawson, J. P. Turkenburg, F. Bjorkling, B. Huge-Jensen, S. A. Patkar, L. Thim, *Nature* **1991**, *351*, 491–494; b) R. Verger, *Trends Biotechnol.* **1997**, *15*, 32–38; c) L. Wang, Y. Lin, Y. Zhou, H. Xie, J. Song, M. Li, Y. Huang, X. Huang, S. Mann, *Angew. Chemie Int. Ed.* **2019**, *58*, 1067–1071.
[19] a) S. Barbe, V. Lafaquière, D. Guieysse, P. Monsan, M. Remaud-Siméon, I. André, *Proteins Struct. Funct. Bioinforma.* **2009**, *77*, 509–523; b) M. Viñambres, M. Filice, M. Marciello, *Polymers (Basel).* **2018**, *10*, 615; c) M. Marciello, J. M. Bolivar, M. Filice, C. Mateo, J. M. Guisan, *Biomacromolecules* **2013**, *14*, 602–607; c) P. Grochulski, Y. Li, J. D. Schrag, F. Bouthillier, P. Smith, D. Harrison, B. Rubin, M. Cygler, *J. Biol. Chem.* **1993**, *268*, 12843–7.
[20] a) R. Rodrigues, J. Ortiz, J. Santos, A. Murcia, A. Alcantara, O. Barbosa. C. Ortiz, R. Lafuente, *Biotech. Adv.*, **2019**, *37*, 746–770; b) M. Filice, O. Romero, A. Aires, J. M. Guisan, A. Rumbero, J. M. Palomo, *Adv. Synt. Cata.*, **2015**, *357*, 2687-2696; c) M. Filice, O. Romero, J. G. Fernández, B. Rivas, J. A. Hermoso, J. M. Palomo. *Chem.Commun.*, **2015**, *51*, 9324-9327; d) J. M. Palomo, M. Filice. *Biotech. Adv.*, **2015**, *33(5)*, 605-613.
[21] B. Thangaraj, P. R. Solomon, *ChemBioEng Rev.* **2019**, *6*, 167–194.
[22] a) M. Filice, J. M. Guisan, M. Terreni, J. M. Palomo, *Nat. Protoc.* **2012**, *7*, 1783–1796; b) J. M. Palomo, M. Filice, O. Romero, J. M. Guisan, **2013**, pp. 255–273.
[23] A. Barth, *Biochim. Biophys. Acta - Bioenerg.* **2007**, *1767*, 1073–1101.
[24] a) F. Secundo. *Chem. Soc. Rev.* **2013**, *42*, 6250-6261; b) M. Hoarau, S. Badieyan, E. Marsh. *Org. Biomol. Chem.*, **2017**,*15*, 9539-9551; c) S.E. Glassford, B. Byrne, S.G. Kazarian. *Biochim. Biophys. Acta.* **2013**, *1834*, 2849-2858.
[25] B. R. Singh, M. P. Fuller, *Appl. Spectrosc.* **1991**, *45*, 1017–1021.
[26] a) P. I. Haris, F. Severcan, *J. Mol. Catal. B Enzym.* **1999**, *7*, 207–221; b) W. K. Surewicz, H. H. Mantsch, D. Chapman, *Biochemistry* **1993**, *32*, 389–394.
[27] S. Krimm, J. Bandekar,*Vibrational Spectroscopy and Conformation of Peptides, Polypeptides, and Proteins;* **1986**, pp. 181–364.
[28] M. Jackson, H. H. Mantsch, *Crit. Rev. Biochem. Mol. Biol.* **1995**, *30*, 95–120.
[29] a) L. K. Tamm, S. A. Tatulian, *Q. Rev. Biophys.* **1997**, *30*, 365–429; b) A. Natalello, D. Ami, S. Brocca, M. Lotti, S. M. Doglia, *Biochem. J.* **2005**, *385*, 511–517.
[30] A. Misiūnas, Z. Talaikytė, G. Niaura, V. Razumas, T. Nylander, *Biophys. Chem.* **2008**, *134*, 144–156.
[31] J.M. Berg, J.L. Tymoczko, L.Stryer. Biochemistry. 5th edition. New York: W H Freeman, ***2002***.
[32] O. Vavra, J. Filipovic, J. Plhak, D. Bednar, S. M. Marques, J. Brezovsky, J. Stourac, L. Matyska, J. Damborsky, *Bioinformatics* **2019**, *35*, 4986–4993.
[33] S. Rehm, P. Trodler, J. Pleiss, *Protein Sci.* **2010**, *19*, 2122–2130.

Entry for the Table of Contents

Insert graphic for Table of Contents here.

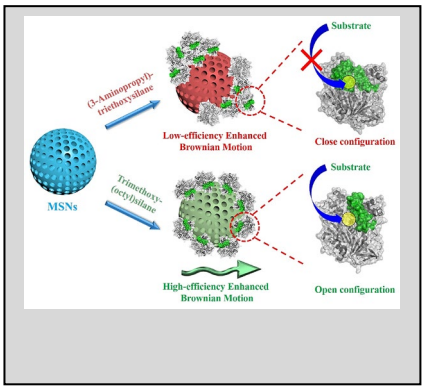

The impact of enzyme orientation on the performance of lipase-powered nanomotors was explored and analysed for the first time, indicating the hydrophobic interaction is the best strategy for immobilizing lipase to provide a high-efficiency catalysis, thus in turn a high-efficiency enhanced Brownian motion, which would be vital in promoting the future applications of enzyme-powered micro/nanomotors.